Physics – Uspekhi **58** (9) 897 – 905 (2015)

CONFERENCES AND SYMPOSIA

PACS numbers: **11.27.+d**, 67.25.dk, 67.30.he

100th ANNIVERSARY OF THE BIRTH OF E M LIFSHITZ

Superfluids in rotation: Landau–Lifshitz vortex sheets vs Onsager–Feynman vortices

G E Volovik

DOI: 10.3367/UFNe.0185.201509h.0970

Contents

Abstract. Landau's and Lifshitz's 1955 paper on vortex sheets in a rotating superfluid came out almost simultaneously with Feynman's paper on quantized vortices in superfluid ^{4}He and was long considered incorrect. Forty years later, in what was a triumph for the authors' theory, experiments at the Olli Lounasmaa Low Temperature Laboratory (Otaniemi, Finland) detected vortex sheets in chiral superfluid ^{3}He-A in a rotating cryostat, validating Landau's and Lifshitz's equation relating the vortex sheet separation and the angular velocity of rotation. This paper discusses vortex sheet configurations that have been or can be observed in superfluid ^{3}He.

Keywords: rotating superfluid, quantized vortices, vortex sheet

G E Volovik Low Temperature Laboratory, Aalto University, P.O. Box 15100, FI-00076 AALTO, Finland
E-mail: volovik@boojm.hut.fi;
Landau Institute for Theoretical Physics, Russian Academy of Sciences, ul. Kosygina 2, 117334 Moscow, Russian Federation

Received 2 April 2015
Uspekhi Fizicheskikh Nauk **185** (9) 970 – 979 (2015)
DOI: 10.3367/UFNr.0185.201509h.0970
Translated by G E Volovik

1. Introduction. Quantized vortices and vortex sheets

Superfluid liquids had been believed to obey the irrotational (potential) flow, $\nabla \times \mathbf{v}_s = 0$. However, experiments by Andronikashvili and Osborne demonstrated the formation of a meniscus in superfluid ^{4}He under rotation. This indicated that this superfluid rotates as a normal liquid, i.e., it participates in the solid body rotation, $\mathbf{v}_s = \mathbf{\Omega} \times \mathbf{r}$, and thus $\nabla \times \mathbf{v}_s = 2\mathbf{\Omega}$. To resolve this puzzle two scenarios were suggested in 1955: one by Feynman [1] and the other by Landau and Lifshitz [2]. In the Feynman approach, solid body rotation on a macroscopic scale is imitated by the array of quantized vortices in Fig. 2a (*right*).

Landau and Lifshitz had another idea. They suggested that irrotational circulating flow was concentrated between the cylindrical vortex sheets (Fig. 1a). Historically, vorticity concentrated in sheets was suggested by Onsager in 1948 [3] and London [4] (see also the vortex sheet in the Onsager notes handwritten in 1945 in Fig. 5 of Ref. [5]). In this arrangement, the flow of the superfluid component also corresponds to the solid body rotation on a macroscopic scale (Fig. 1b). By minimizing the energy of the rotating liquid $F = 1/2\rho_s(\mathbf{v}_s - \mathbf{v}_n)^2 V + \sigma A$ (where ρ_s is the density of the superfluid component of the liquid, $\mathbf{v}_s - \mathbf{v}_n$ is the velocity of the superfluid component with respect to the normal component, V is the volume of the cell, σ is the surface tension, and A is the area of the vortex sheet), Landau and

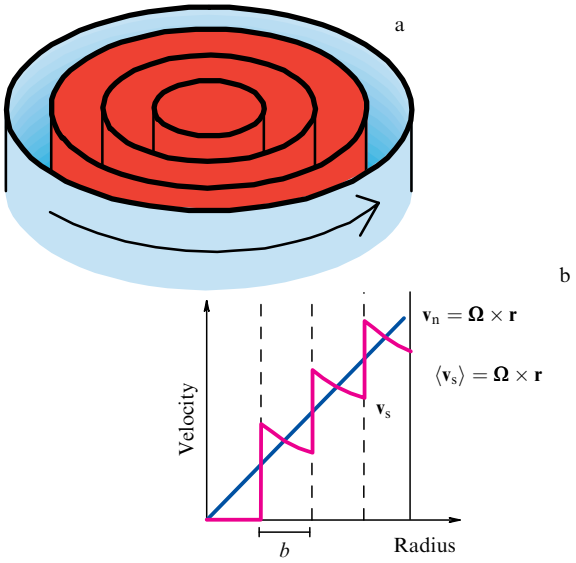

Figure 1. Vortex sheet scenario by Landau–Lifshitz (1955). Due to cylindrical vortex sheets (a), the potential flow of the superfluid component between the sheets simulates the solid body rotation of a liquid on average (b). The distance b between sheets as a function of angular velocity Ω of rotation is found by minimization of the energy of the rotating liquid, which includes the kinetic energy of the flow and surface tension of the tangential discontinuity on the vortex sheet.

Lifshitz calculated the spacing b between the neighboring vortex sheets:

$$b = \left(\frac{3\sigma}{\rho_s \Omega^2} \right)^{1/3}, \qquad (1)$$

where Ω is the angular velocity of rotation.

The surface tension of the tangential discontinuity in superfluid ^{4}He was estimated by Ginzburg [6], and the effective density of the superfluid involved in rotation together with vortex sheets was calculated by I M Lifshitz and M I Kaganov [7].

2. Vortex sheet instability in superfluid ^{4}He

It turned out, however, that in superfluid ^{4}He the vortex sheet scenario does not work for several reasons. First, the tangential discontinuity is unstable against the breakup of the sheet into separate pieces (Fig. 2b), which finally transform into the quantized vortex lines in Fig. 2a (*right*).

Then, there is the problem of the formation of such a state of a rotating liquid. A system of equidistant layers may exist only at sufficiently high velocity $\mathbf{\Omega}$ of rotation. How are they formed when we start rotation and increase the angular velocity from zero? According to Landau and Lifshitz, first, a small cylindrical sheet must appear in the center of the container. However, we know now that objects with sharp inhomogeneity are not easily created in the bulk liquid: they appear at the wall of the container and then propagate to the bulk. This would mean that as angular velocity increases, more and more elementary cylindrical sheets penetrate into the rotating vessel. They will not merge to form larger cylinders, because at high velocities the array of small sheets appears to be energetically more favorable than the system of coaxial sheets. All this suggests that the scenario of coaxial vortex sheets may never occur.

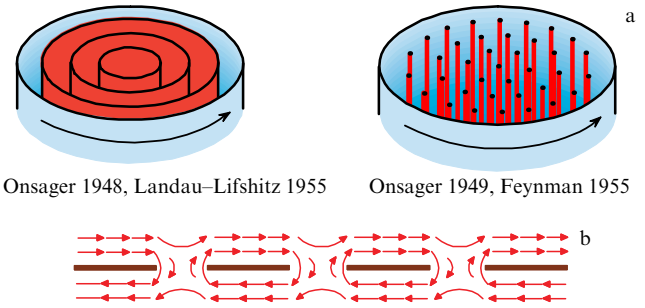

Figure 2. Vortex sheet is unstable in superfluid ^{4}He against the formation of vortex lines. The tangential discontinuity is unstable against the breakup of the sheet into separate pieces (b), which form quantized vortex lines (a *right*).

Nevertheless, though the Landau–Lifshitz scenario was not applicable to the trivial superfluidity in liquid ^{4}He, this idea turned out to be correct for chiral superfluid ^{3}He-A. First, the vortex sheet there is locally stable against decay into segments, since it is based on the topologically protected soliton. Second, the sheet is formed from the boundary of the container. And finally, though the system of small cylinders and the system of quantized vortices are energetically more favorable, they cannot form in the process of the adiabatic growth of the vortex sheet state.

The Landau–Lifshitz equation (1) for distance between the vortex sheets as a function of Ω has been experimentally confirmed in NMR measurements, which was the triumph of the theory. The Bragg reflection from the locally equidistant sheet planes has also been found [8].

3. Continuous vorticity in chiral superfluid ^{3}He-A. Skyrmions and merons

The chiral Weyl superfluid ^{3}He-A is an orbital ferromagnet with magnetization along the orbital angular momentum $\hat{\mathbf{l}}$ of a Cooper pair [9]. Simultaneously, it is the spin antiferromagnetic (spin nematic) with anisotropy axis $\hat{\mathbf{d}}$ which allows us to investigate the properties of ^{3}He-A using the NMR technique.

Typical vortices, which appear in ^{3}He-A under rotation, are continuous vortices — textures without singularity in the order parameter field (Fig. 3a). The structure of the $\hat{\mathbf{l}}$-field in the continuous vortex is similar to the structure of skyrmions — topologically twisted continuous field configurations in quantum field theory [10]. The topological winding number of the skyrmion texture gives rise to the quantized circulation of superfluid velocity around the skyrmion [11]. A skyrmion represents the vortex with two quanta of circulation ($N = 2$), i.e., the phase of the order parameter changes by 4π when circling the vortex. Vortex-skyrmions have been experimentally identified in ^{3}He-A in NMR experiments [12]. Skyrmion lattices were later discovered also in magnetic materials [13].

A skyrmion can be represented as a molecule which consists of two radicals, called merons. Each meron has the circulation number $N = 1$ (the 2π-vortex). Due to topological reasons, under the conditions of NMR experiments, an isolated meron cannot exist in a bulk liquid. That is why merons are combined to molecules and form skyrmions.

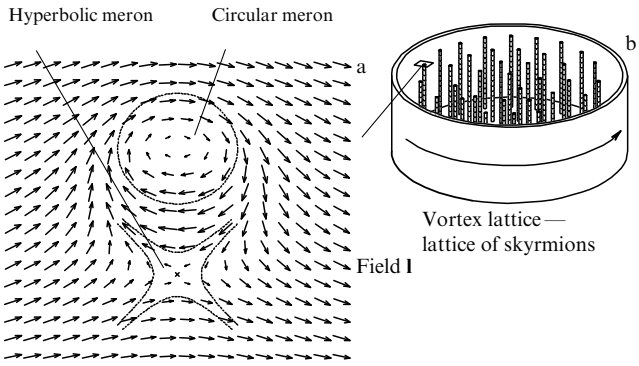

Figure 3. Superfluid ^{3}He-A is an orbital ferromagnet with magnetization along the orbital angular momentum $\hat{\mathbf{l}}$ of a Cooper pair and simultaneously the spin antiferromagnetic (spin nematic) with anisotropy axis $\hat{\mathbf{d}}$. Typical vortices, which are created in ^{3}He-A under rotation, are continuous vortices with 4π winding of the condensate phase around the vortex (two quanta of circulation). The vorticity is generated by texture in the ferromagnetic field $\hat{\mathbf{l}}$, which is called a skyrmion. The skyrmion can be represented as the bound state of two merons, circular and hyperbolic. Each meron represents a vortex with a single quantum of circulation (the so-called Mermin–Ho vortex [11]). In the center of the circular vortex-meron the vector $\hat{\mathbf{l}}$ is parallel to $\mathbf{\Omega}$, while in the center of the hyperbolic vortex-meron the vector $\hat{\mathbf{l}}$ is antiparallel to $\mathbf{\Omega}$.

4. Solitons and merons

The other possibility of the existence of merons is within the core of the topological soliton. The topological $\hat{\mathbf{l}}$-soliton in superfluid ^{3}He-A (Fig. 4a) looks similar to the Bloch or Neel wall in ferromagnets. However, as distinct from the domain wall one can make the hole in the soliton wall by the formation of the half-quantum vortex ($N = 1/2$) (see Fig. 11 in Section 10). Meron represents the kink in the $\hat{\mathbf{l}}$-soliton (Fig. 4b). It separates two parts of the soliton with the opposite winding. The solitonic meron looks similar to the Bloch line within the Bloch wall in ferromagnets [16]; it cannot exist outside the soliton in the same manner as the Bloch line cannot escape from the domain wall.

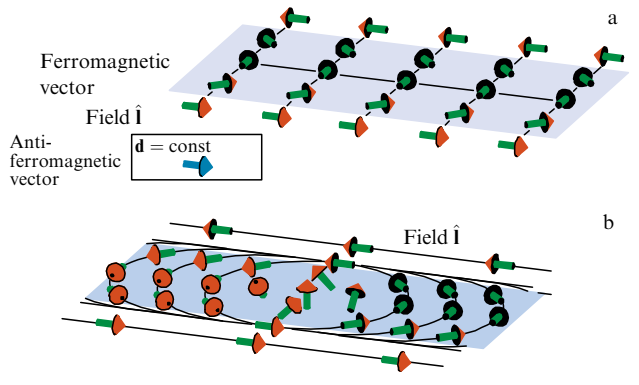

Figure 4. (Color online.) (a) Topological $\hat{\mathbf{l}}$-soliton in superfluid ^{3}He-A is the analog of the Bloch or Neel wall in ferromagnets. The ferromagnetic vector $\hat{\mathbf{l}}$ changes the direction to the opposite across the soliton, while the antiferromagnetic vector $\hat{\mathbf{d}}$ remains constant. The $\hat{\mathbf{l}}$-soliton is characterized by the nontrivial element of the Z_2 relative homotopy group. As distinct from the domain wall, the soliton can terminate on a singular topological defect — the half-quantum vortex ($N = 1/2$). The phase of the condensate changes by π around such a vortex [14, 15] (see Section 11, Fig. 11). (b) The meron is similar to the Bloch line within the Bloch wall in ferromagnets. In a chiral superfluid, meron represents the 2π vortex ($N = 1$).

For us it is important that merons carry the quantum of vorticity, $N = 1$, and thus they serve as the building blocks for construction of vortex sheets, which have been experimentally investigated in superfluid ^{3}He-A [8, 17, 18].

5. Vortex sheet as a chain of merons

When the topologically stable soliton accumulates vorticity in the form of merons with the same circulation number $N = 1$, it forms the vortex sheet (Fig. 5c). The vortex sheet has a hierarchy of length scales [19, 20]. On a macroscopic scale, the planes of the vortex sheets have a local order of the smectic liquid crystal (Fig. 5a). The neighboring planes of the vortex sheet are separated by layers with the vortex-free superflow (Fig. 5b).

According to the Landau–Lifshitz theory, the vortex sheets allow for the solid-body like rotation of the superfluid on a macroscopic scale, i.e., with the average velocity field obeying equation $\langle \mathbf{v}_s \rangle = \mathbf{\Omega} \times \mathbf{r}$, and thus $\langle \nabla \times \mathbf{v}_s \rangle = 2\mathbf{\Omega}$.

6. Growth of the folded vortex sheet. Theory

Numerical simulation of the growth of the vortex sheet [19] is shown in Fig. 6. From experimental observations, it follows that once the vortex sheet appears in the cell, the critical velocity of the formation of new merons is substantially smaller (about 6–7 times) than the critical velocity of the formation of the doubly quantized ($N = 2$) vortex-skyrmions. Merons have a small critical velocity for creation, because the soliton is always in close contact with the side wall. New merons are created at the edges of the soliton on the wall and then easily enter the soliton. That is why the further acceleration of the angular velocity leads to the growth of the soliton rather than to the creation of new skyrmions. In the final state of such adiabatic growth, the skyrmions are absent, while a multiply folded vortex sheet is formed, which locally simulates the coaxial sheets of Landau–Lifshitz (see Fig. 6e). Note that in this figure the maximal number of merons was $N = 226$, while in experiments N can reach 10^3, where the coaxial cylindrical structure of the folded vortex sheet is more pronounced. A similar structure has been recently suggested for the vortex sheet in multi-component Bose condensates [21].

The number of merons in the vortex sheet depends on angular velocity Ω of the rotating vessel. For large Ω the number of vortices-merons $N(\Omega)$ in the cell approaches the value $N_0(\Omega) = (2m/\hbar)\,\Omega R^2$, where m is the mass of the ^{3}He atom. This function $N_0(\Omega)$ does not depend on the surface tension of the soliton: it corresponds to the solid body rotation of the superfluid component, $\langle \nabla \times \mathbf{v}_s \rangle = 2\mathbf{\Omega}$.

7. Planar vortex sheet

For small Ω, the finite size effect is present: the surface tension of the soliton becomes important, and as a result the meron number is smaller than that which corresponds to the macroscopic solid body rotation of the liquid, $N(\Omega) < N_0(\Omega)$. Note that the vortex sheet itself performs the solid body rotation together with the container, but the flow of the whole liquid does not follow the solid body rotation. The same deficit of the effective density of the liquid involved in rotation was considered by I M Lifshitz and M I Kaganov [7] for Landau–Lifshitz concentric sheets.

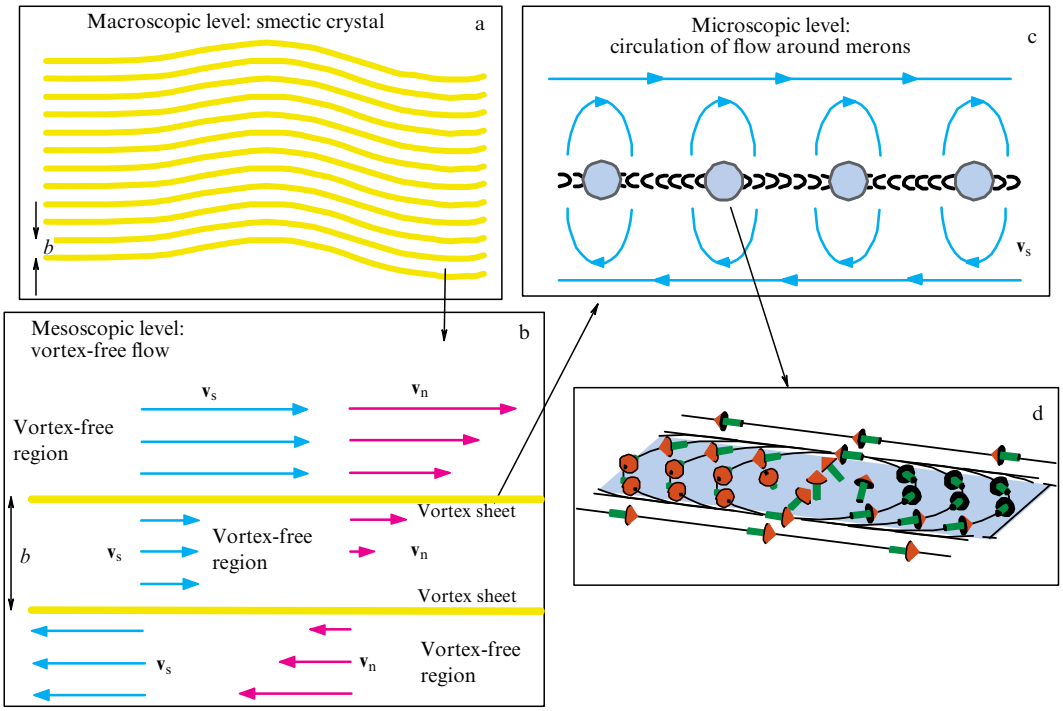

Figure 5. (Color online.) Vortex sheet structure. (a) On a macroscopic scale, the planes of the vortex sheets form a local order of the smectic liquid crystal. (b) Flow velocity fields of superfluid and normal components between the sheet planes. In these regions, the superflow is vortex-free (superfluid velocity is constant), while the velocity of the normal component $\mathbf{v}_n = 2\Omega y\hat{\mathbf{x}}$ (where the y-axis is normal to the plane of the vortex sheet, and $\hat{\mathbf{x}}$ is the unit vector along the axis in the plane of the sheet). (c) Flow velocity field of the superfluid component around merons (Mermin–Ho vortices with $N = 1$). (d) Structure of an individual circular meron.

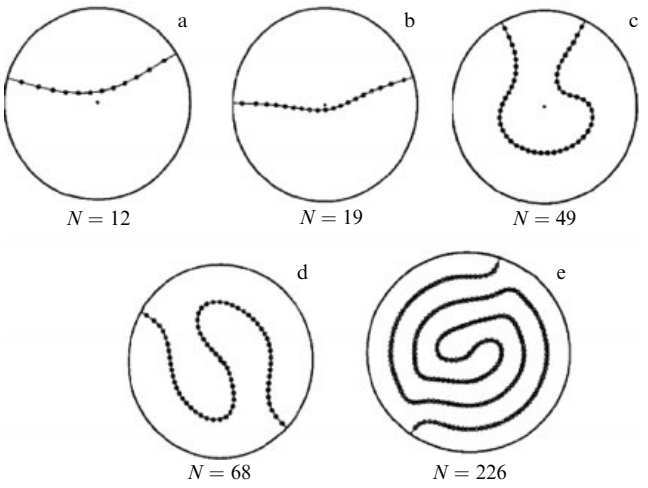

Figure 6. Vortex sheet is formed in a rotating vessel if a topological soliton is for some reason present in the container. With increasing Ω, merons enter the soliton from the side wall, and a folded vortex sheet is formed. The numerical simulation of the growth of the vortex sheet with adiabatically increasing angular velocity of rotation Ω is shown. N is the number of merons on the sheet. In the range $12 < N < 19$, the vortex sheet has the form of a plane along the diameter of the cylinder (see Fig. 7). For large Ω, the configuration approaches that of Landau–Lifshitz cylindrical vortex sheets, but these sheets are connected. In this limit, the dependence of the number of vortex-merons $N(\Omega)$ on angular velocity approaches the function $N_0(\Omega) = (2m/\hbar)\,\Omega R^2$, which does not depend on the surface tension of the soliton and corresponds to the equilibrium number of the isolated vortices in the rotating container.

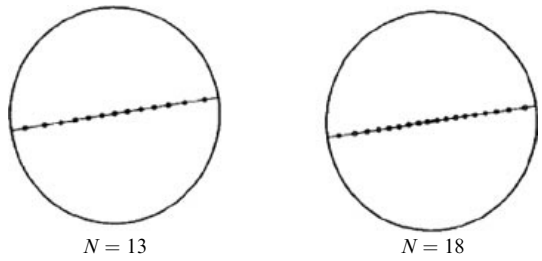

Figure 7. Straight vortex sheet is formed in the interval $12 < N < 19$. The meron number $N(\Omega)$ in this configuration does not depend on the soliton tension, since the area of the soliton does not change within this interval. Eqn (4) gives $N(\Omega) = 0.42N_0(\Omega)$.

There is a range of velocities, where the equilibrium configuration of the vortex sheet is represented by merons accumulated by a straight soliton along the diameter of the cylinder (the plane which contains the axis of the cylinder). In Fig. 6, this is the range $12 < N < 19$. For the straight soliton, the function $N(\Omega)$ can be found analytically.

Let x be the coordinate along the straight soliton with $x = 0$ on the axis of the container and $n(x)$ the density of vortex-merons in the soliton (the 2π-vortices). If one neglects the image forces from the boundary, the equation for $n(x)$ is

$$\frac{\hbar}{2m}\int_{-R}^{R} \mathrm{d}y\,\frac{n(y)}{x-y} = \Omega x\,. \qquad (2)$$

This corresponds to the solid body rotation of the soliton (the soliton is stationary in the rotating frame if superflow velocity produced by other vortices at the place of a given meron is equal to the solid body velocity $v_y = \Omega x$). The soliton surface tension does not enter the equation, since the length of the soliton is always the same, $L = 2R$. Equation (2) has the

solution

$$\frac{\hbar}{2m}\, n(x) = \frac{\Omega}{\pi}\sqrt{R^2 - x^2}\,. \tag{3}$$

The total number of merons is $N = \int \mathrm{d}x\, n(x) = N_0/2$. The boundary effects are taken into account by adding the auxiliary vortices. With vortex images, Eqn (2) transforms into

$$\frac{\hbar}{2m}\int_{-R}^{R} \mathrm{d}y\, n(y)\left(\frac{1}{x-y} - \frac{1}{x - R^2/y}\right) = \Omega x\,, \tag{4}$$

which gives $N \approx 0.42 N_0$.

8. NMR signature of vortex sheets

The properties of different textures in ^{3}He-A (solitons, vortices, and vortex sheets) are investigated using NMR (see, e.g., review papers [20, 22]). The cores of these topological objects produce the potential wells for the spin wave (magnon) in Fig. 8a. The excitation of magnons in the bound state gives rise to a satellite peak in the NMR absorption spectrum at a frequency below the main peak (Fig. 8b). The position of the satellite peak indicates the type of object, while the intensity of the peak gives information on the size of the object or on the number of the identical objects.

If the rotating state represents an array of vortex-skyrmions, the intensity is proportional to the number of vortices, and thus is linear in Ω (Fig. 8c) (triangles). In the vortex sheet state of rotation, the NMR absorption in terms of Ω is close to the $\Omega^{2/3}$ law (Fig. 8c) (squares and circles). This is consistent with the Landau–Lifshitz equation (1): since the area of the soliton is $A = V/b$, where V is the volume of the cell, from Eqn (1) we obtain $A \propto \Omega^{2/3}$.

In the vortex-sheet state, the measured absorption is 1.5–3 times higher than in a pure vortex-skyrmion state (Fig. 8c). The vortex sheet produces the potential well for magnons, the area of which per one quantum of circulation is larger than the area of the core of a skyrmion.

9. Bragg peak as signature of the layered structure of vortex sheets

Locally, the folded vortex sheet represents equidistant layers, and thus has a local order of the smectic liquid crystal (Fig. 5a). In NMR experiment, this periodic structure is manifested by the Bragg peak in Fig. 9. The measured distance b between the sheets (see inset in Fig. 9) is in good agreement with the Landau–Lifshitz equation (1), where the known values of the superfluid density and the soliton tension are used.

10. Formation of the vortex sheet. Experiment

In experiments, the vortex sheet is reproducibly created during the sinusoidal modulation of velocity $\Omega = \Omega_0 \sin(\omega t)$ (see Fig. 10, bottom). The period of modulation is usually $T = 2\pi/\omega \approx 10$ s. The vortex sheet appears if the amplitude Ω_0 of modulation exceeds some critical velocity which is slightly above the critical velocity for the nucleation of the skyrmions. This means that the formation of the vortex sheet is related to the presence of skyrmions in the cell. During multiple and fast alterations of the angular velocity of the container, the skyrmions cannot maintain the equilibrium arrangement corresponding to a momentary angular velocity $\Omega(t)$. They are pressed to the side wall of the container, where their mutual collapse gives rise to a small seed of the soliton attached to the surface of the container.

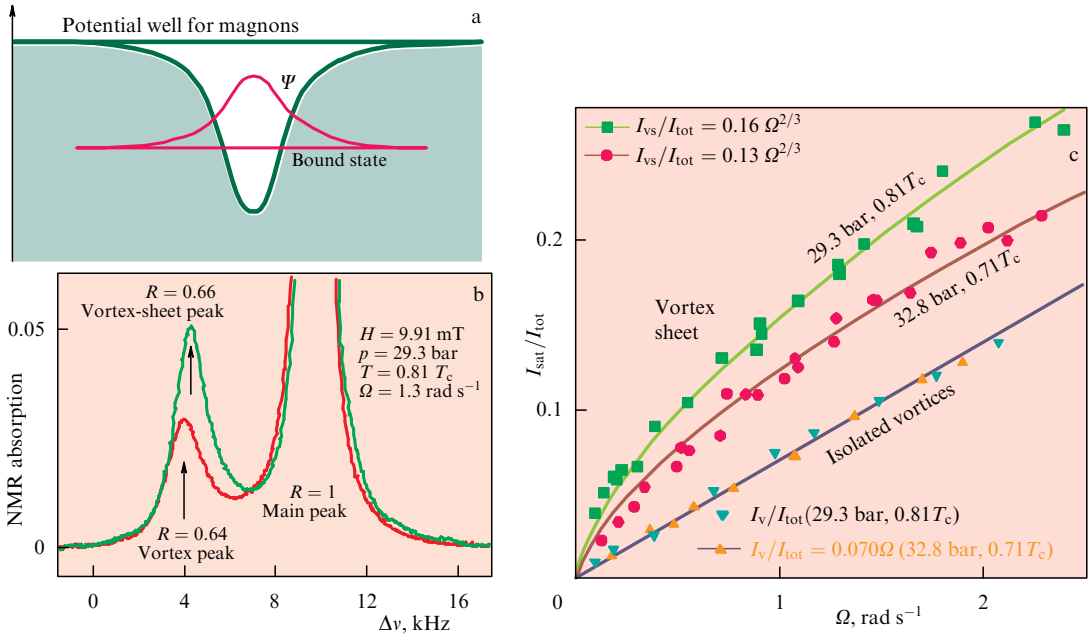

Figure 8. (Color online.) NMR absorption on skyrmions and on the vortex sheet. (a) The core of the skyrmion and the soliton represent, correspondingly, the two-dimensional and one-dimensional potential wells for spin waves — magnons. In NMR experiments, the bound states of magnons in these potentials are excited. This corresponds to the satellites in the NMR spectrum on the lower frequency side of the main peak (b). The vortex sheet state has higher absorption than the lattice of isolated skyrmions, since the area of the soliton is larger than the area of the vortex cores. (c) Intensity of the satellite peak as a function of the angular velocity Ω of rotation. In the vortex lattice state, the intensity is proportional to the number of vortices, $N_0(\Omega) = (2m/\hbar)\,\Omega R^2$, and thus is linear in Ω. In the vortex sheet state, the intensity is proportional to the area of the soliton, and thus to $\Omega^{2/3}$, which agrees with the Landau–Lifshitz equation.

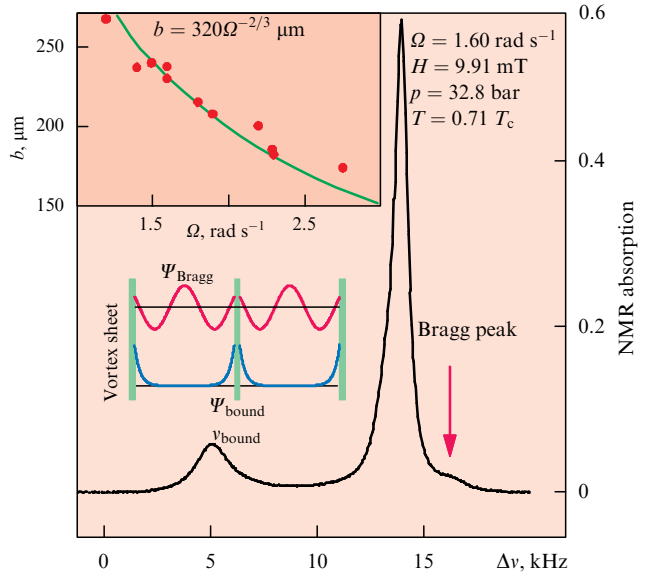

Figure 9. (Color online.) Bragg peak in the NMR spectrum on the higher frequency side of the main peak. It corresponds to the Bragg reflection satellite from the standing spin waves between neighboring sheets and allows us to measure the distance between the sheets. (inset) The experimental values for the distance $b(\Omega)$ between the sheets (circles) is in agreement with the Landau–Lifshitz equation (1) within a 10% accuracy (solid line).

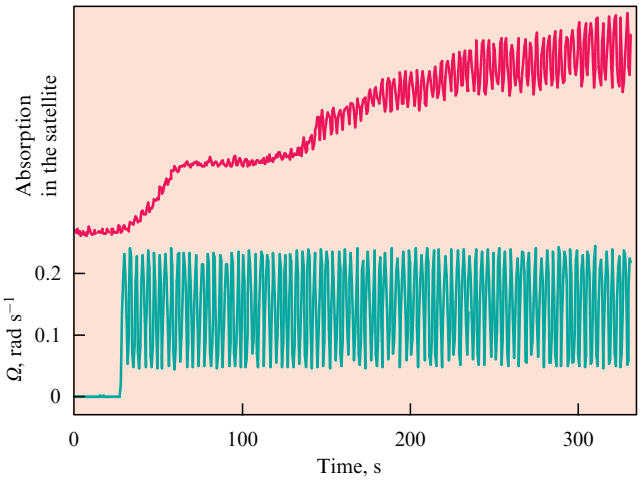

Figure 10. (Color online.) Modulation of angular velocity Ω (*bottom*). A straight soliton is formed by periodic oscillation of the container. The formation of this soliton is indicated by a plateau in the absorption (*top*), since the area of a straight soliton does not depend on the number of merons. After the straight soliton is formed, the folded vortex sheet is obtained by adiabatic growth of the soliton by gradually increasing the rotation velocity.

Whatever the dynamical reason is for the nucleation of the soliton seed, once the soliton is created, the further process is fully determined. The critical velocity for entering a new vorticity — merons — in the soliton from the wall is substantially smaller than the critical velocity for the creation of isolated vortex-skyrmions. The soliton grows by absorbing new merons which enter the soliton from the wall. The soliton with accumulated merons forms a folded vortex sheet connected to the side wall and at large Ω imitates Landau–Lifshitz cylindrical sheets.

The upper frame of Fig. 10 displays the absorption in the satellite as a function of time. At the beginning of modulation, the increase in the absorption is small and corresponds to nucleation of a few separate continuous vortices. After 2.5 minutes, the first seed of the vortex-soliton is created and develops within ≈ 20 s to a constant level, where there is no sinusoidal structure in absorption. This corresponds to the formation of the straight soliton in Fig. 7. During a periodic drive the absorption remains constant, because the area of the vortex sheet does not change. The intensity of the satellite also agrees with the straight soliton. Numerical simulation shows that the straight shape of the vortex sheet is the stable configuration in a certain window of the meron number N in the soliton: $12 < N < 19$ (Fig. 7) [19].

When Ω is increased further and exceeds some critical value, the straight soliton becomes unstable against the curved one. At larger N and Ω, the length of the soliton grows and finally the folded vortex sheet sweeps the whole cell to produce a homogeneous distribution of merons, which on average imitates the solid body rotation of a superfluid, $\langle \mathbf{v}_s \rangle = \mathbf{\Omega} \times \mathbf{r}$. Instead of one scale which characterizes the intervortex distance in the conventional vortex array, the vortex sheet is characterized by two scales: intervortex distance within the sheet and the mean distance b between the neighboring parts of the curved soliton.

11. Topological stability of the vortex sheet

The topological stability of both the soliton and the kinks (merons) inside the soliton prevents the vortex sheet from breaking into individual vortices, and thus the sheet is extended from one boundary of the container to another. In principle, the soliton can terminate in a bulk, but in this case the termination line represents the half-quantum vortex [14]. This is the object with a singular core of the coherence length size (hard core), which is the counterpart of the Alice string in high energy physics and of an object with one half of the magnetic flux quanta observed in high temperature superconductors [15].

A hole can be made in the soliton sheet, with the boundary of the hole being the closed loop of the half-quantum vortex (Fig. 11). If the radius of the loop exceeds critical value on the order of the soliton thickness (~ 10 μm), it will be energetically advantageous for the vortex ring to grow and destroy the whole vortex sheet. In superfluid ^{3}He-B, hard-core vortices of a similar size have been produced by neutron irradiation [23].

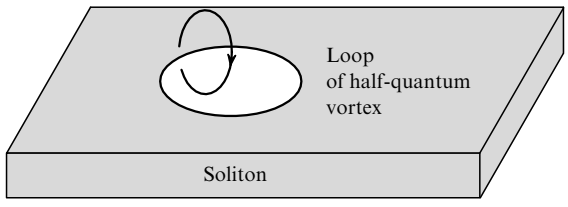

Figure 11. Stability of a vortex sheet. The vortex sheet is based on the topological soliton. As distinct from the ferromagnetic domain walls, it is possible to drill a hole in the soliton. Such a hole is bounded by the topological line defect, a string loop, where the string is the half-quantum vortex (vortex with winding number $N = 1/2$). If a vortex loop with a radius exceeding the critical value on the order of the thickness of the soliton wall (~ 10 μm) is created, the loop will further grow and destroy the whole vortex sheet. It is known that neutron irradiation produces hot spots (micro Big-Bang [23]) of the proper size, but all attempts to destroy the vortex sheet by neutron irradiation failed.

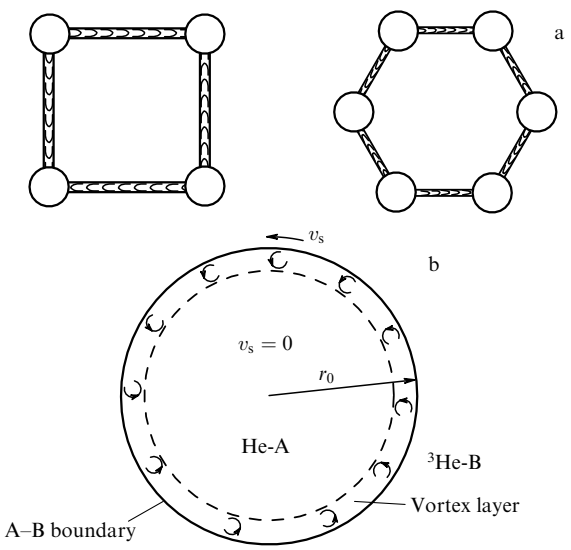

Figure 12. Multiple vortices. Closed vortex sheets represent N-quantum vortices. (a) Vortex sheets with $N = 4$ and $N = 6$ merons in ^{3}He-A. The radius of the N-quantum vortex is determined by the balance of forces: the repulsive interaction between the vortex-merons is compensated by the attraction due to surface tension of the soliton [see Eqn (7)]. (b) Multiply quantized vortex in ^{3}He-B. Vorticity in the form of the vortex sheet can be concentrated at the interface between ^{3}He-B and the cylindrical domain of ^{3}He-A [25] (see also Section 14 and Fig. 14d).

So we tried to produce the half-quantum vortices in ^{3}He-A in a similar way in order to make a hole in the vortex sheet. However, irradiation by neutrons and by γ-quanta for several hours could not destroy the vortex sheet.

12. Cylindrical vortex sheets as multiply quantized vortices

There are many possible equilibrium configurations of the rotating chiral superfluid ^{3}He-A, which produce the solid body rotation of the liquid on a macroscopic scale. Practically all of them (including the array of vortex-skyrmions) are metastable. But if they are somehow created, they live practically forever due to the extremely large energy barriers compared with temperature. The main problem is to find the proper way to prepare the particular configuration. There are many topological objects which have still evaded observation, because the scenarios for their creation and stabilization have not been found. Among them are the half-quantum vortex [1] and multiply quantized vortices [24].

The vortex sheet provides the possibility of constructing multiply quantized vortices [24]. A closed vortex sheet with N merons represents the N-quantum vortex. Since the $N = 2$ vortex is the known vortex-skyrmion, and the odd number of merons in the closed vortex sheet is prohibited by the topology, the multiply quantized vortices start with $N = 4$ (Fig. 12).

For large N ($N \gg 1$), the multiply quantized vortex is the cylindrical vortex sheet. Its radius r_N is obtained by minimization of the superflow energy outside the vortex and the energy of the soliton wall:

$$E_N = \pi\rho_s \frac{\hbar^2}{4m^2} N^2 \ln\frac{R}{r_N} + 2\pi\sigma r_N , \qquad (5)$$

[1] Just recently the observation of the half-quantum vortices in the polar phase of superfluid ^{3}He has been reported [33]. (*Added in English proof.*)

where R is the radius of the cell. Minimization gives

$$r_N = N^2 \frac{\hbar^2\rho_s}{8m^2\sigma} . \qquad (6)$$

For small N (but for $N > 3$), the cylinder should be substituted by a polyhedron — an N-gonal prism (Fig. 12). The radius of the prism is determined by the balance of forces: the repulsive interaction between vortices is compensated by the attraction due to surface tension of the soliton:

$$r_N = \frac{\pi(N-1)}{\sin(\pi/N)} \frac{\hbar^2\rho_s}{8m^2\sigma} . \qquad (7)$$

Within an order of magnitude, Eqns (6) and (7) also give a correct estimate of the core size of the skyrmion in Fig. 3, which consists of $N = 2$ merons.

13. Multiple sheets

Though the array of small cylindrical sheets is energetically more favorable than the folded vortex sheet, we failed to produce and stabilize such a system. For that, it is necessary to construct the proper disturbance on the container wall, which makes the creation of the cylindrical walls easier than the creation of skyrmions or vortex sheets connected to the wall.

Instead, a way was found to split the folded vortex sheet into several pieces, which are connected to the side wall of the container. The splitting occurs when the original single sheet is subjected to a high-frequency modulation with a large amplitude [26] (Fig. 13). The obtained structure is determined by the dynamics of the merons. The narrow hysteresis loop in Fig. 13 corresponds to multiple sheets which are formed after modulation $\Omega(t) = 1.2 + 0.4\sin(\omega t)$, with $2\pi/\omega = 10$ s. The response of the short sheets is faster than that of the folded sheet, since with the radial alignment of the sheets it is easier for merons to enter and escape the soliton during the fast modulation of angular velocity.

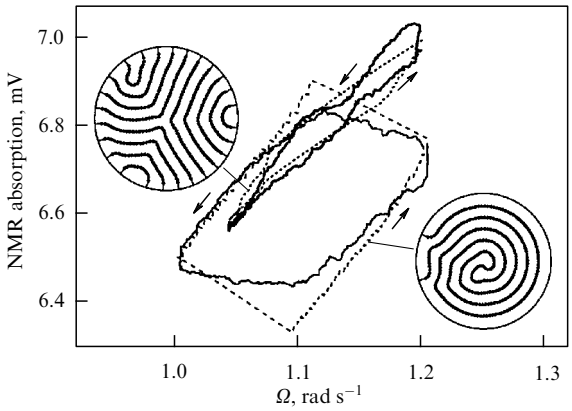

Figure 13. Selection of rotating states by fast dynamics. The hysteresis loop in the state with the multiple vortex sheets (thick solid line) is narrow compared to that in the state with a single folded sheet (thin solid line). In other words, the multiple sheets have much faster dynamics than the folded sheet. That is why the multiple sheets are better adjusted to the rotation if the rotation is accompanied by rapid oscillations. The dotted lines show the results of numerical simulations for the configuration with multiple sheets (*left inset*) and for the configuration with an adiabatically grown folded sheet (*right inset*).

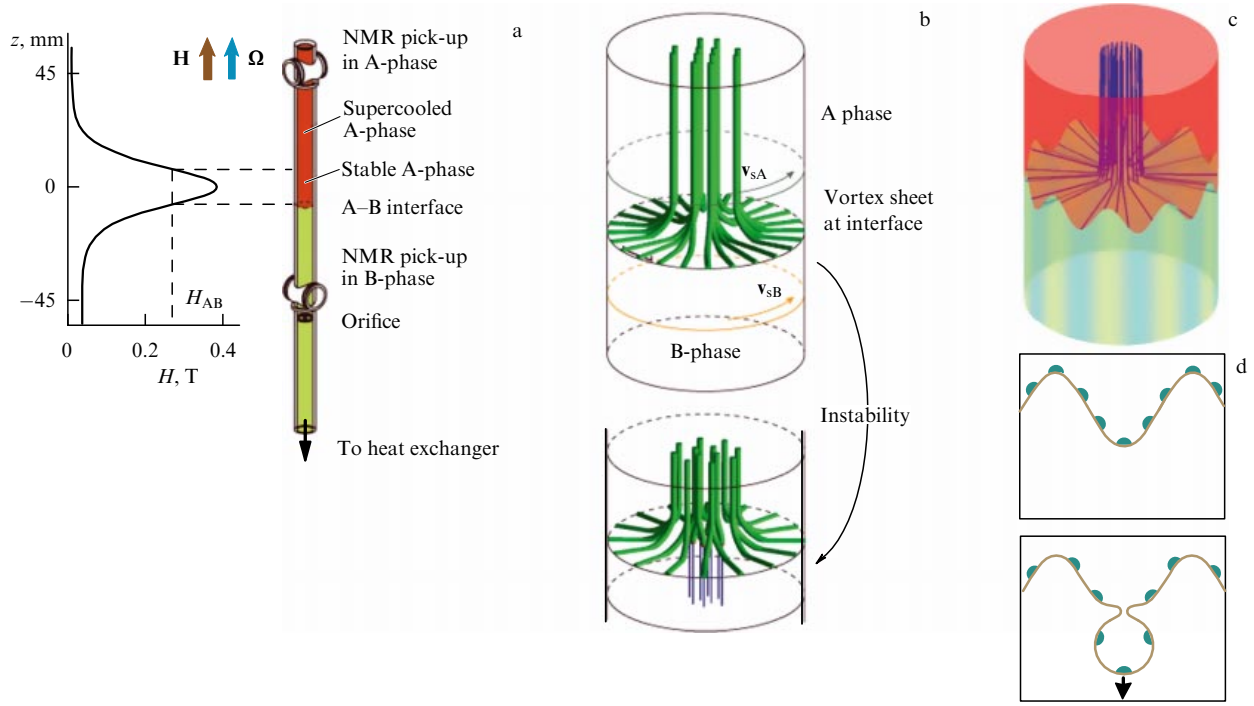

Figure 14. (Color online.) Vortex sheet at the interface between rotating ^{3}He-A and vortex-free ^{3}He-B. (a) Experimental cell. The enhanced magnetic field at $z = 0$ prohibits propagation of the B-phase into the upper part of the cell. (b) The vortex-full A-phase is separated from the vortex-free B-phase by the vortex sheet, which is concentrated at the A–B interface. That is why the interface serves as a tangential velocity discontinuity. (c) When the velocity jump across the interface reaches the critical value, ripples are formed (analogs of wind-generated surface waves). (d) The development of the instability leads to the formation of a droplet of the vortex sheet inside the B-phase. Such a sheet is unstable to the formation of quantized B-phase vortices (b).

14. Vortex sheet at the A–B interface

A crucial property of ^{3}He superfluids is the existence of several length scales. In particular, the core size of the vortex-skyrmion in ^{3}He-A is 10^3 times larger than the core size of quantized vortices in ^{3}He-B. Sharp (hard-core) vortices are not easily created: the critical velocity of the vortex nucleation under rotation is inversely proportional to the core radius [27]. As a result, one can prepare a state in the rotating cryostat in which the A-phase skyrmion lattice simulates the macroscopic solid body rotation of a superfluid, while the B-phase is still in the static vortex-free state, which is called the Landau state. A-phase vortex-skyrmions cannot penetrate from the A- to the B-phase, so they form a surface vortex sheet at the phase boundary [28] (Fig. 14b, *top*). Vortex sheets which appear in the mixture of several superfluids have been discussed in Ref. [25] (see the cylindrical vortex sheet in Fig. 12b and in Ref. [29]).

The vortex sheet in Fig. 14b (*top*) separates two superfluids moving with respect to each other. Near the boundary of the container, the jump in the tangential velocity reaches $|v_A - v_B| = \Omega R$. This arrangement brings a lot of interesting physics.

If the velocity difference $|v_A - v_B|$ exceeds the critical value, the interface experiences instability against the generation of surface waves — ripplons (analogs of the capillary-gravitational waves in conventional liquids) (Fig. 14c). The onset of the analog of the Kelvin–Helmholtz instability is marked by the appearance of vortex lines in ^{3}He-B, which are detected in NMR measurements [30]. At the non-linear stage of the instability, a droplet of the vortex sheet is formed (Fig. 14d, *bottom* and Fig. 12b). This droplet propagates into the B-phase, where the vortex sheet splits into singly quantized vortices, which form the vortex cluster in Fig. 14b (*bottom*). The formation of vortices in the B-phase after the discussed development of instability allowed us to measure in NMR experiments the value of the critical velocity and compare it with the theory.

It appeared that the measured threshold of the instability is lower than that for the classical Kelvin–Helmholtz instability, and instead it satisfies the Landau critical velocity for the radiation of ripplons (see details in [31] and in book [15, Ch. 27]). In the shallow water limit, the radiation of ripplons above the threshold corresponds to the Zel'dovich–Starobinsky effect of radiation of electromagnetic waves by rotating black holes (Ref. [15, Ch. 31]).

15. From vortex sheet to quantum turbulence

Formation of B-phase vortices due to the instability of the surface vortex sheet allows us to use this phenomenon as the working tool for injection of vortices into the vortex-free B-phase under rotation. The injection of a few vortices into a superfluid in its metastable vortex-free Landau state revealed a new phenomenon in quantum turbulence [32]. The NMR measurements after injection demonstrated a sharp transition to turbulence. At temperatures above $0.60T_c$ (where T_c is the transition temperature for superfluidity), the flow of the superfluid is regular (laminar): the injected vortices form a small cluster in the center of the cell (Fig. 14b, *bottom* and Fig. 15a). However, below $T < 0.60T_c$, a turbulent behavior is observed: vortices are multiplied in the turbulent regime and finally fill the whole region of the B-phase (Fig. 15b).

Surprisingly, the observed sharp transition to turbulence is insensitive to the fluid velocity. This is in striking contrast to classical turbulence regulated by the Reynolds number

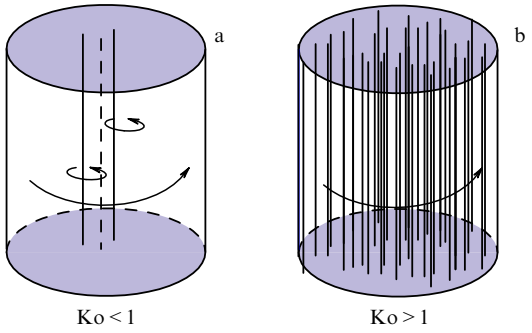

Figure 15. (Color online.) Results of the injection of a few vortices into ^{3}He-B after the development of vortex sheet instability at the A–B interface in Fig. 14d. The final state of ^{3}He-B under rotation depends on the value of Kopnin number Ko(T) — the temperature dependent analog of the Reynolds number, which characterizes the quantum turbulence. As distinct from the Reynolds number in classical liquids, the Kopnin number does not contain the velocity of the liquid. For $\mathrm{Ko}(T) < 1$, the injected vortices form a small cluster in the center of the container. For $\mathrm{Ko}(T) > 1$, the injected vortices are multiplied, forming a chaotic vortex flow, which fills the whole cell. Finally, the turbulent vorticity relaxes to the equilibrium lattice of the rectilinear vortices, which imitates the solid body rotation of the B-phase.

$\mathrm{Re} = UR/\nu$, which is proportional to the velocity U of the liquid. Quantum superfluid turbulence is controlled by an intrinsic parameter of the superfluid: the Kopnin number Ko, which is the ratio of the reactive and dissipative parameters in the equations for superfluid hydrodynamics, which depends only on temperature T.

In Fermi superfluids, such as superfluid ^{3}He and superconductors, the Kopnin number $\mathrm{Ko} \sim \omega_0\tau$, where ω_0 is the minigap — the distance between the levels of Andreev-Majorana fermions in the core of the vortex — and τ is their lifetime. For $\mathrm{Ko}(T) < 1$, the effect of chiral anomaly (spectral flow) provides a momentum exchange between vortices and the normal component of the liquid. In this regime, dissipation dominates, and the flow of the superfluid component is laminar. For $\mathrm{Ko}(T) > 1$, the effect of the inertial term dominates, and the laminar flow becomes unstable against turbulence.

16. Conclusion

The vortex sheet structure of a rotating superfluid was calculated by Landau and Lifshitz in 1955. In 1995, i.e., 40 years later, it was experimentally demonstrated that for complex superfluids with the multi-component order parameter this concept was instrumental. The Landau–Lifshitz vortex sheet proved to be an important physical object with nontrivial topology and with many physical applications.

Acknowledgements
This work was supported in part by the Academy of Finland (project No. 250280) and by the facilities of the Cryohall infrastructure of Aalto University.

References

1. Feynman R P "Application of quantum mechanics to liquid helium", in *Progress in Low Temperature Physics* Vol. 1 (Ed. C J Gorter) (Amsterdam: North-Holland, 1955) p. 17
2. Landau L D, Lifshitz E M "On the rotation of liquid helium" *Dokl. Akad. Nauk SSSR* **100** (4) 669 (1955)
3. Onsager L (unpublished); see: London F *Superfluids* Vol. 2 (New York: Wiley, 1954) p. 151
4. London H, in *Report of an Intern. Conf. on Fundamental Particles and Low Temperatures, Cambridge, England, 22 – 27 July 1946* Vol. 2 (London: The Physical Society, 1947) p. 48
5. Eyink G L, Sreenivasan K R *Rev. Mod. Phys.* **78** 87 (2006)
6. Ginzburg V L "The surface energy associated with a tangential velocity discontinuity in helium II" *Sov. Phys. JETP* **2** 170 (1956); "O poverkhnostnoi energii, svyazannoi tangentsial'nym razryvom skorosti v gelii II" *Zh. Eksp. Teor. Fiz.* **29** 254 (1955)
7. Lifshits I M, Kaganov M I "The effective density of rotating liquid helium II" *Sov. Phys. JETP* **2** 172 (1956); *Zh. Eksp. Teor. Fiz.* **29** 257 (1955)
8. Parts Ü et al. *JETP Lett.* **59** 851 (1994); *Pis'ma Zh. Eksp. Teor. Fiz.* **59** 816 (1994)
9. Vollhardt D, Wölfle P *The Superfluid Phases of Helium-3* (London: Taylor and Francis, 1990)
10. Skyrme T H R *Nucl. Phys.* **31** 556 (1962)
11. Mermin N D, Ho T-L *Phys. Rev. Lett.* **36** 594 (1976)
12. Seppälä H K et al. *Phys. Rev. Lett.* **52** 1802 (1984)
13. Mühlbauer S et al. "Skyrmion lattice in a chiral magnet" *Science* **323** 915 (2009)
14. Volovik G E, Mineev V P *JETP Lett.* **24** 561 (1976); *Pis'ma Zh. Eksp. Teor. Fiz.* **24** 605 (1976)
15. Volovik G E *The Universe in a Helium Droplet* (Oxford: Clarendon Press, 2003)
16. Dedukh L M, Nikitenko V I, Sonin E B *Sov. Phys. Usp.* **28** 100 (1985); *Usp. Fiz. Nauk* **145** 158 (1985)
17. Parts Ü et al. *Phys. Rev. Lett.* **72** 3839 (1994)
18. Eltsov V B et al. *Physica B* **284 – 288** 252 (2000)
19. Heinilä M T, Volovik G E *Physica B* **210** 300 (1995)
20. Thuneberg E V *Physica B* **210** 287 (1995)
21. Simula T P et al. *J. Phys. Soc. Jpn.* **80** 013001 (2011)
22. Salomaa M M, Volovik G E *Rev. Mod. Phys.* **59** 533 (1987)
23. Ruutu V M H et al. *Nature* **382** 334 (1996)
24. Volovik G E, Krusius M *Priroda* (4) 56 (1994)
25. Volovik G E, Misirpashaev T Sh *JETP Lett.* **51** 537 (1990); *Pis'ma Zh. Eksp. Teor. Fiz.* **51** 475 (1990)
26. Eltsov V B et al. *Phys. Rev. Lett.* **88** 065301 (2002)
27. Parts Ü et al. *Europhys. Lett.* **31** 449 (1995)
28. Hänninen R et al. *Phys. Rev. Lett.* **90** 225301 (2003)
29. Kasamatsu K, Tsubota M *Phys. Rev. A* **79** 023606 (2009)
30. Blaauwgeers R et al. *Phys. Rev. Lett.* **89** 155301 (2002)
31. Volovik G E *JETP Lett.* **75** 418 (2002); *Pis'ma Zh. Eksp. Teor. Fiz.* **75** 491 (2002)
32. Finne A P et al. *Nature* **424** 1022 (2003)
33. Autti S, Dmitriev V V, Eltsov V B, Makinen J, Volovik G E, Yudin A N, Zavjalov V V, "Observation of half-quantum vortices in superfluid ^{3}He", arXiv:1508.02197